Freshwater transport from warm to cold ocean regions amplifying faster than all model estimates

Taimoor Sohail (t.sohail@unsw.edu.au)
University of New South Wales

Jan Zika
UNSW Sydney https://orcid.org/0000-0003-3462-3559

Damien Irving
Commonwealth Scientific and Industrial Research Organisation (CSIRO)

John Church
University of New South Wales

Physical Sciences - Article

Keywords: water cycles, global ecosystems, global evaporation

Posted Date: July 24th, 2021

DOI: https://doi.org/10.21203/rs.3.rs-723246/v1

Version of Record: A version of this preprint was published at Nature on February 23rd, 2022. See the published version at https://doi.org/10.1038/s41586-021-04370-w.

Freshwater transport from warm to cold ocean regions amplifying faster than all model estimates

Taimoor Sohail[1], Jan D. Zika[1], Damien B. Irving[2], and John A. Church[3]

[1]School of Mathematics and Statistics, University of New South Wales, Sydney, Australia
[2]Commonwealth Scientific and Industrial Research Organisation (CSIRO), Hobart, Australia
[3]Climate Change Research Centre, University of New South Wales, Sydney, Australia

July 16, 2021

Abstract

Warming-induced global water cycle changes pose a significant challenge to global ecosystems and human society. The magnitude of historical water cycle change is uncertain due to a dearth of direct rainfall and evaporation observations, particularly over the ocean where 80% of global evaporation occurs. Air-sea fluxes of freshwater and river run-off imprint on ocean salinity at different temperatures, such that warmer regions tend to be saltier and cooler regions tend to be fresher. In this work, we track observed salinity trends in the warm, salty fraction of the ocean from 1970 to 2014, and infer the global poleward transport of freshwater over this period. Since 1970, $46 - 77 \times 10^{12}$ m^3 of freshwater has been transported poleward from the warmest fraction of the ocean. No model in the current generation of climate models (the 6th Climate Model Intercomparison Project; CMIP6) replicates this transport, with the closest model underestimating transport by $2 - 4$ times. We trace the climate model biases to a weaker than expected surface freshwater flux intensification, just $0 - 4\%$ in CMIP6 models compared to an estimated $3 - 7.5\%$ in observations.

The global water cycle represents the sustained transport of freshwater through the lithosphere, hydrosphere, biosphere and atmosphere, and underpins the foundation of human society and ecological systems. Understanding the response of the global water cycle to long-term global warming is critically important to preparing for and mitigating the impacts of climate change. However, direct observations of rainfall are sparse, particularly over the ocean, which acts as a conduit for 80% of global freshwater transport [1, 2]. Limited rainfall and evaporation observations, combined with substantial variance across atmospheric reanalysis products [3, 4] have made direct measurements of long-term changes to the global water cycle challenging. As a result, much of our understanding of changes to the water cycle over the past fifty years has been shaped by proxies for rainfall measurements over the ocean including salinity. As water associated with the hydrological cycle transits through the ocean, it generates a signature of ocean salinification (where evaporation changes exceed precipitation and river runoff changes) and freshening (where precipitation and river runoff changes exceed evaporation changes), both at the surface [5, 6] and the interior [7, 8]. Using in-situ observations and modelling of ocean salinity, a growing body of research has identified a 'wet gets wetter, dry gets drier' paradigm, wherein the global water cycle intensifies due to global warming [9, 5, 10], with some estimates suggesting a water cycle intensification of $2 - 4\%$ relative to the 1950 ocean state [8, 6, 11]. This intensification manifests as increasingly salty sub-tropical oceans and increasingly fresh tropical and sub-polar oceans.

The observed distribution of salinity change (or tendency) in the global ocean has a large scale coherent pattern through depth and between ocean basins (see figure 1). While the Indo-Pacific basin has coherent regions of freshening and salinification, the Atlantic basin is broadly salinifying in warmer temperature zones (compare figures 1a and b with figures 1c and d). There are also significant differences between observational estimates of ocean salinity changes (figures 1a and c) and climate model outputs over the same period (figures

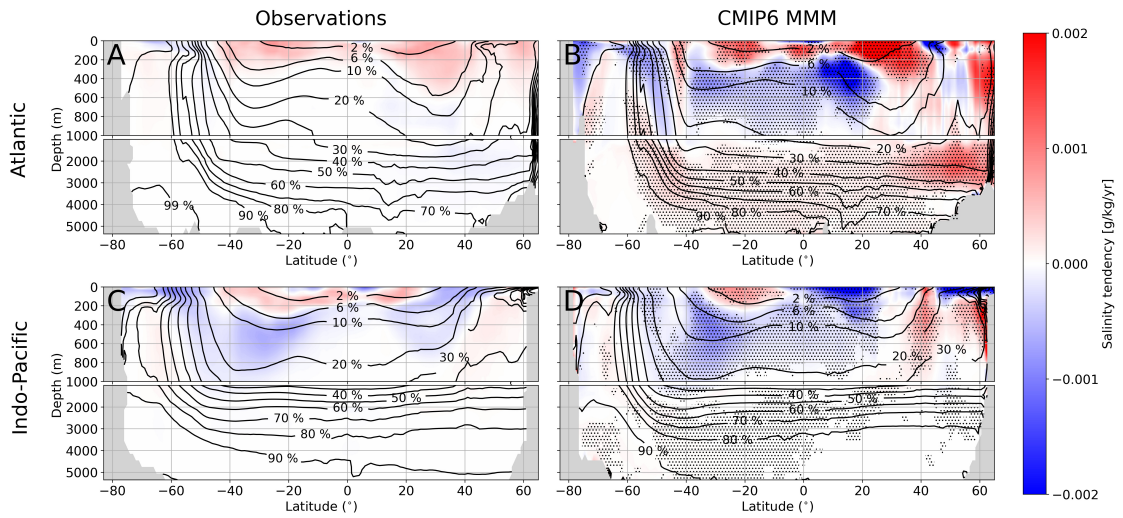

Figure 1: Zonally-averaged salinity tendency, in $g/kg/year$, in a) composite observations (IAP and EN4) in the Atlantic and c) the Indo-Pacific basins, and b) and d) in the CMIP6 multi-model mean (MMM). Stippling in b) and d) indicates regions where more than 2/3 of the CMIP6 models agree on the sign of the salinity tendency. Black contour lines indicate zonally averaged 'temperature-percentiles' with the warmest 2% of the ocean bound by the 2% contour, the warmest 6% by the 6% contour and so on. Here we track salinity changes within these percentile layers.

1b and d). Salinity changes appear to roughly align along contours of constant temperature (black contour lines in figure 1). Based on this realisation, past research has used water mass-based diagnostics to frame ocean salinity changes, for instance, by quantifying mean salinity in temperature (or density) layers (known as the 'T–S' curve of the ocean) [12, 7, 13].

Tracking the T–S curve over time provides information about global salinity changes while maintaining the ability to differentiate between climatic regions using temperature. However, simply computing trends of absolute salinity (S) at constant conservative temperature (T) ignores ocean warming which moves the underlying T-S curve. [14]. Indeed, as the ocean warms, the coldest temperatures in the sub-polar and polar oceans will disappear, while new tropical waters will be created, so a trend at constant T can be misleading. In this work, we analyse salinity changes at constant 'temperature-percentile' rather than constant temperature [15]. That is, we organise the ocean from warmest to coldest and track changes at fixed accumulated volume. For example, by tracking salinity changes within the warmest 6% of the ocean volume, we are able to track a region which retains the same volume and remains in roughly in the same climatic region even as the ocean warms. This framework allows us to track changes in the T–S curve of the ocean while eliminating much of the direct influence of ocean warming. The overlaid black contours in figure 1 illustrate the geographical distribution of temperature-percentiles in the observations, from hot (0%) to cold (100%). Past research has used temperature-percentiles to analyse heat content change, revealing that approximately 50% of surface heat flux changes enter 90% of the ocean volume via the sub-polar ocean since 1970 [15].

Changes to the T–S curve may be attributed to changes in the build up of greenhouse gases (GHGs) and aerosols in the atmosphere. GHGs tend to accelerate the warming of the climate system, thereby amplifying the strength of the water cycle in a 'wet-gets-wetter-dry-gets-drier' pattern [10, 4]. Anthropogenic and natural aerosols, on the other hand, tend to cool the climate system on a global scale, leading to the opposite response in the water cycle, with wet areas getting drier and dry areas getting wetter [10]. In essence, aerosols tend to homogenise latitudinal bands of rainfall and evaporation over the globe, while GHGs tend to intensify the contrast between such regions. Forcing climate models solely by anthropogenic aerosols or by GHGs provides a wider range of water cycle perturbations by which to judge climate model responses. This spread of model

responses may consequently be useful in understanding sources of biases across the current generation of historical climate simulations.

Our temperature-percentile framework is not impacted by the amount of warming a model experiences as everything is normalised into percentiles, and thus may be used to address a number of long-standing questions surrounding global hydrological cycle changes. In this work, we track changes in conservative temperature and absolute salinity in three gridded hydrographic historical observations (IAP, Ishii and EN4 [16, 17, 18]), as well as changes in potential temperature and practical salinity in twenty Climate Model Intercomparison Project - Phase 6 (CMIP6) historical model runs and six Detection and Attribution Model Intercomparison Project (DAMIP) historical model runs (see Methods for theory and data sources). We also evaluate a fourth, composite observational data set (referred to as 'Composite Observations') which combines IAP data where depth $z < 2000$ m and EN4 data where $z > 2000$ m. This data set is formulated to limit salinity errors associated with sampling biases prior to the Argo era (see [16] for information on IAP sampling biases and [15] for further information on the composite data set). All observational and model data sources except Ishii cover the historical period from 1970 to 2014, with Ishii covering the period from 1970 to 2012. Using these observations and models, we produce an estimate of observed poleward freshwater transport since 1970 and explore biases in salinity trends in the latest generation of climate models.

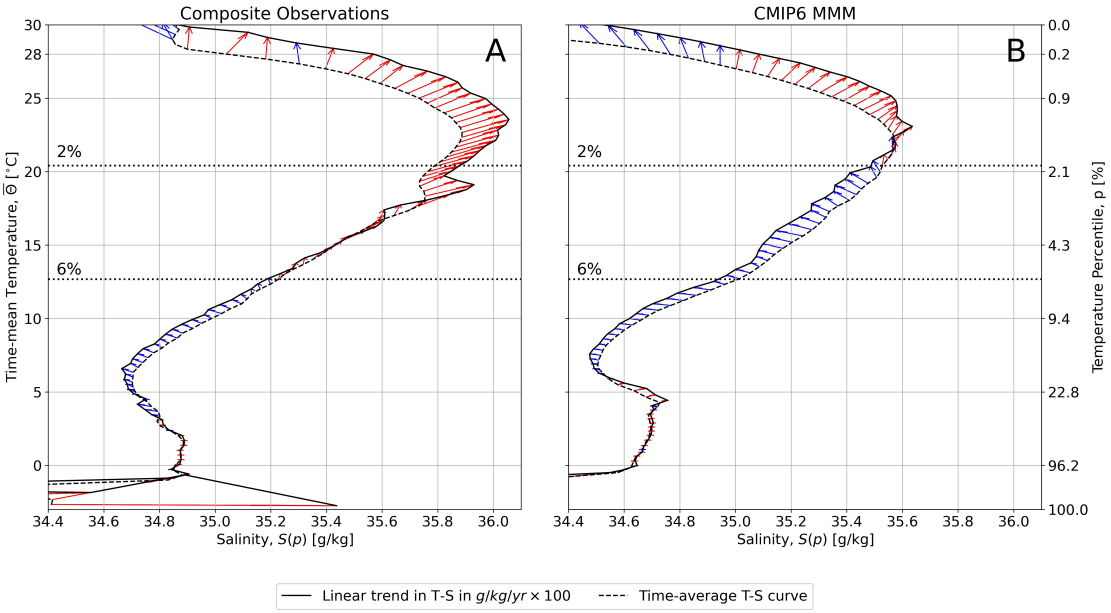

Figure 2: Linear trend in the global T–S curve $[g/kg/yr \times 100]$, in a) observations, and b) the CMIP6 multi-model mean (MMM). The right-hand y-axis shows the corresponding accumulated temperature-percentile in observations. The y-component of the arrow vectors is the change in temperature at constant temperature-percentile and the x-component is the change in salinity. Red implies salinification and blue implies freshening.

The time-mean T–S curve (dashed black curve in figure 2) has a characteristic '?' shape. Mean ocean salinity is lowest at the warmest and coldest temperature-percentiles (representing the tropics, sub-polar and polar regions), and is highest at an intermediate temperature-percentile range (representing the sub-tropics). The observed salinity tendency follows the widely established 'wet-gets-wetter-dry-gets-drier' pattern (figure 2a), with red arrow vectors showing salinification in the sub-tropics (between the warmest 0.2% – 6% of the ocean) and blue vectors exhibiting freshening in the tropics (the warmest 0% – 0.2% ocean by volume) and sub-polar/polar regions (the warmest 6% – 100% ocean by volume). The CMIP6 multi-model mean projections exhibit salinification over a much narrower band of temperature-percentiles, between the warmest

0.2% – 2% of the ocean. Note that the CMIP6 models largely conserve salt on a global scale (see figure S3a, S3b and [19]), as do observations within the range of uncertainty presented.

In addition to the global T–S changes presented here, we may also refer to the basin-scale salinity tendencies in figure 1 to explore hemispheric shifts in salinity. Indeed, figure 1 reveals a pattern of freshwater transport from the North Atlantic to the North Pacific in both models and observations, with a stronger transport in CMIP6 models compared to observations. Based on figure 2, the warmest 2% of the ocean experiences salinfication in both the CMIP6 model and observations, and the warmest 6% of the ocean experiences salinification in the observations. Consequently, we focus hereafter on tracking changes in the warmest 2% and warmest 6% of the ocean.

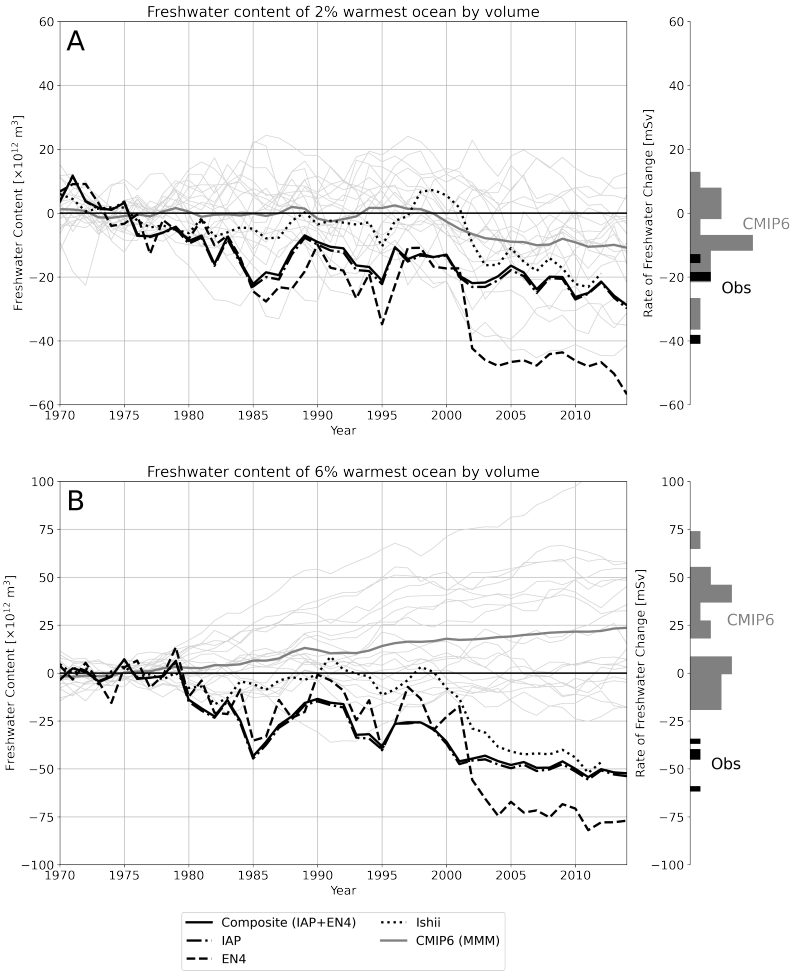

Figure 3: The change in freshwater content in a) the warmest 2% of the ocean and b) the warmest 6% of the ocean, relative to a 1970-1980 baseline, in all observational data sets and CMIP6 model runs. Histograms show the rate of freshwater change (in mSv) of each model member and observational product based on the slope of a linear regression over the historical period.

In order to account for the volume of ocean water that experiences salinification in the observations and models, we multiply mean salinity by layer volume to obtain a global freshwater content (as in equation (6) in Methods). In the warmest 2% ocean by volume (figure 3a), the freshwater content decreases in both the observations and the CMIP6 models, relative to a 1970-1980 baseline. By the end of the historical period, the warmest 2% of the ocean has lost 1.7 – 5.2 times more freshwater in the observations than in

the CMIP6 ensemble mean. That said, the rate of freshwater change in some CMIP6 models (calculated as the slope of the linear regression over the historical period) is the same as that in three out of four of the observational data sets (histograms in figure 3a). In the warmest 6% of the ocean (figure 3b), the observed ocean loses substantially more freshwater than the CMIP6 models. Overall, the observations suggest a poleward redistribution of freshwater of between 46 and 77×10^{12} m^3. On the other hand, many CMIP6 models (and the CMIP6 ensemble mean) experience a freshening over the historical period, with the closest CMIP6 model experiencing a freshwater loss of about 1/3 of observations (18×10^{12} m^3). There is also larger spread between individual model realisations, with the models coalescing into two distinct groups (histograms in figure 3b). A 'salty' group experiences little to no freshwater change over the historical period, while a 'fresh' group experiences freshening over the same period. The specific models which correspond to each group are listed in Table S1 in the supplementary information.

Note that the difference between models and observations in the warmest 6% of the ocean may be due to a difference in the *pattern* of salinity change rather than a difference in *magnitude* of salinity change. Figure 1 shows the magnitude of salinity change in the CMIP6 models is in fact greater than that in the observations, but in the models a freshening signal intrudes into the 6% warmest ocean by volume in the North Atlantic and North Pacific, which may be the cause of the difference in freshening between the observations and the CMIP6 models in figure 3. Future projections of warming-induced extreme precipitation and global agricultural changes are based in part on estimates of water cycle change from CMIP6 models. That CMIP6 models cannot accurately capture historical salinity trends is therefore a cause of concern for future climate change projections.

The systematic fresh bias in CMIP6 models must be urgently addressed in order to provide accurate future climate projections. In order to sample a wider range of perturbations to the water cycle, we compare a set of six DAMIP models that each performed a historical greenhouse gas forcing only (GHG-only) and a historical anthropogenic aerosol forcing only (AA-only) experiment with their corresponding CMIP6 historical response. Since GHGs tend to intensify the water cycle and AAs tend to weaken the water cycle over time, comparing water cycle intensification in the DAMIP models with the change in ocean freshwater content may provide some information about the cause of the freshwater content bias. In the warmest 2% of the ocean, there is a correlation between surface flux intensification (as a percentage of the pre-industrial freshwater transport) and freshwater content change, with an r-squared value of 0.51 (figure 4a). As the water cycle over the warmest 2% of the ocean intensifies, the freshwater content in this volume decreases. Applying a linear regression across the DAMIP runs and their six corresponding CMIP6 historical runs (red, purple and blue dots) to the observed freshwater content change, we estimate the the water cycle has intensified by 3 – 12% in the warmest 2% of the ocean (green shaded area in figure 4a). This water cycle amplification estimate lies closer to the cloud of DAMIP and CMIP6 models than the warmest 6% of the ocean implying that the model response is somewhat realistic (keeping in mind the small observational sample size). In the warmest 6% of the ocean, the linear regression also indicates an inverse relationship between water cycle amplification and freshwater content, with an r-squared value of 0.43. However, the observational estimate of surface flux intensification (3 – 7.5%) lies broadly outside the cloud of DAMIP and CMIP6 models (0 – 4%). Thus, in the warmest 6% of the ocean, we conclude that the surface flux intensification in the CMIP6 models is too weak and as a consequence the models are biased fresh. While this relationship is based on six models rather than the wider suite of twenty CMIP6 models analysed earlier, we note that the response in the fourteen other CMIP6 models (small black dots in figure 4) lies in broadly the same region as the six CMIP6 historical runs corresponding to the DAMIP models (purple dots in figure 4). This implies that the correlations obtained here may be applicable across all CMIP6 models. Note that while the correlation between surface flux changes and freshwater content changes identified in figure 4 holds for the 2 and 6% warmest ocean by volume studied here, mixing and circulation changes do play a role in the warm tropics and at colder temperatures (see figure S3 in supplementary information).

Our understanding of global water cycle changes hinges on a clear understanding of historical water cycle changes, and on climate models' faithful reproduction of these changes. In this study, we quantify the poleward redistribution of freshwater since 1970, inferred from gridded ocean observations. Between 1970

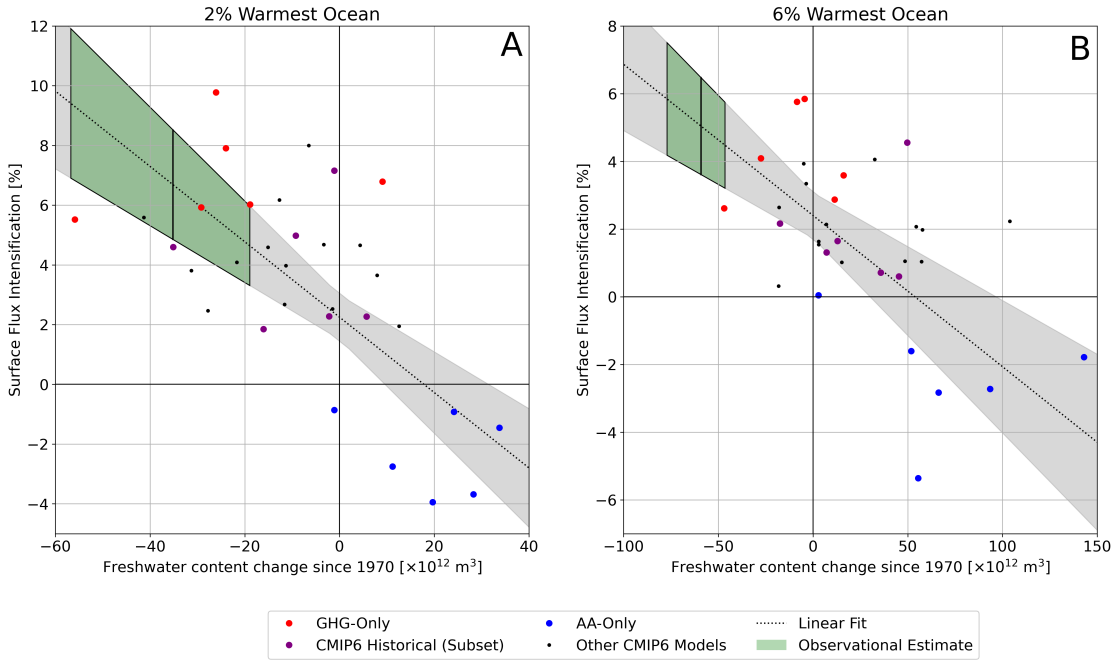

Figure 4: The relationship between surface freshwater flux intensification (relative to pre-industrial surface freshwater fluxes) and freshwater content changes (relative to a 1970 – 1980 baseline) in the DAMIP GHG-only, AA-only and corresponding six CMIP6 historical runs (red, blue and purple dots, respectively), in a) the warmest 2% of the ocean and b) the warmest 6% of the ocean. Small black dots show the broader suite of fourteen other CMIP6 historical simulations. The dotted line represents the linear regression across the DAMIP runs and their corresponding CMIP6 historical runs, and the grey shaded region shows the error associated with the linear regression. The green shaded region is an estimate of surface flux intensification based on the (known) observed freshwater content change and the linear regression. The vertical black line in the green shaded area is an estimate of surface flux intensification based on the mean change in observed freshwater content.

and 2014, we estimate that $46 - 77 \times 10^{12}$ m^3 of freshwater has been transported towards the poles.The latest generation of climate models, collectively called CMIP6, show broad inter-model variability in poleward freshwater transport, which is at best 2 – 4 times smaller than the observations. The CMIP6 models experience salinification over a narrower band of temperatures, calling into question the accuracy with which they may be able to produce future water cycle projections. The consistent salinification bias in CMIP6 models may be explained by surface flux biases, specifically, we postulate that water cycle amplification may be too weak in CMIP6 historical runs, resulting in a weaker than expected freshening trend. These results have profound consequences on current studies relying on CMIP6 models to understand water cycle changes and the associated environmental and societal consequences, and warrant further exploration of the surface freshwater fluxes in climate models.

Acknowledgements

We acknowledge the World Climate Research Programme, the CMIP6 and DAMIP climate modeling groups, the Earth System Grid Federation (ESGF), and the funding agencies supporting CMIP6, DAMIP and ESGF. Modeling and analysis were undertaken with National Computational Infrastructure (NCI) facilities, supported by the Australian Government. This work is supported by the Australian Research Council (ARC) Centre of Excellence for Climate Extremes, the Centre for Southern Hemisphere Oceans Research (a joint

197 research centre between the QNLM and the CSIRO) and the ARC Discovery Project scheme (DP190101173).

Methods

Theory

The tracer-percentile framework

We begin by touching upon the formulation for the tracer-percentile framework in temperature-percentiles, as laid out in detail by [15]. The volume of ocean warmer than a given conservative temperature Θ^* is expressed as:

$$\mathcal{V}(\Theta^*, t) = \iiint_{\Theta(x,y,z,t)>\Theta^*} dxdydz, \tag{1}$$

where Θ is the global temperature field and Θ^* is the binning temperature chosen for the integration. We invert equation (1) to express temperature as a function of volume, $\mathcal{V}$, or equivalently, temperature-percentile, p:

$$\mathcal{V}(\Theta^*, t) \Longleftrightarrow \Theta(\mathcal{V}, t) \equiv \Theta(p, t), \tag{2}$$

where $p = \mathcal{V}/V_T \times 100$ and V_T is the total volume of the ocean. $\Theta(\mathcal{V}, t)$ therefore represents the mean temperature bounding a given volume, and $\Theta(p, t)$ represents the mean temperature bounding a given temperature-percentile. The total volume of the ocean changes negligibly over time, so the volume and temperature-percentile in this framework are related by a constant factor.

Mean salinity in temperature-percentiles

We now extend the tracer-percentile framework by deriving the mean tracer tendency budget at constant tracer-percentile. In this case, the mean tracer of interest is mean salinity, but this framework may be readily modified for use with other conservative and non-conservative tracers. The mean salinity at constant temperature is defined as:

$$S(\Theta^*, t) = \frac{\partial}{\partial \Theta^*}\left(\frac{\partial \Theta^*}{\partial \mathcal{V}}\right) \iiint_{\Theta(x,y,z,t)>\Theta^*} S(x, y, z, t) dxdydz, \tag{3}$$

where $S(x, y, z, t)$ is the three-dimensional absolute salinity field in the ocean. To find mean salinity at temperature-percentiles, we interpolate $S(\Theta^*, t)$ onto $\Theta(p, t)$ surfaces:

$$S(\Theta^*, t) \Longrightarrow S(\Theta(p, t), t) = S(p, t). \tag{4}$$

Mapping mean salinity changes at constant temperature-percentiles ensures we maintain the benefits of adiabatic-invariant watermass methods while also being able to trace freshwater fluxes directly to climatic regions (e.g., tropics, sub-tropics and sub-polar regions) at the ocean's surface.

The resulting variable $S(p, t)$ provides a characteristic $p - S$ curve for the ocean which, like T–S curves, captures changes in the salinity distribution of the global ocean [12]. For ease of comparison with traditional T–S curves, we recast the $p - S$ curve onto the time-mean temperature $\overline{\Theta}(p)$ for a given temperature-percentile, yielding a 'remapped' T–S curve.

Freshwater content and fluxes in temperature-percentiles

In order to account for the volume of water in a given percentile layer experiencing salinity changes, we calculate a freshwater content, $F(p, t)$ by multiplying salinity by layer volume:

$$F(p, t) = \frac{0.01 p V_T}{S_0}(S(p, t) - \overline{S}(t)), \tag{5}$$

where $\overline{S}(t)$ is the volume-averaged salinity that serves as the baseline differentiating 'fresh' and 'salty' water in the ocean, and S_0 is the reference salinity, assumed to be $S_0 = 35$ g/kg. The global change in freshwater, or freshwater flux $\mathcal{F}(p,t)$, can be expressed as:

$$\mathcal{F}(p,t) = \frac{0.01 p V_T}{S_0} \frac{\partial S}{\partial t}(p,t), \tag{6}$$

In practice, $\partial S/\partial t$ is approximated over the time period of interest as the slope of the linear trend in $S(p,t)$. $\mathcal{F}(p,t)$ is related to surface fluxes $\mathcal{F}_s$ and local fluxes of salt in the ocean, $\mathcal{M}$, including mixing, such that the freshwater tendency budget may be defined as $\mathcal{F} = \mathcal{F}_s + \mathcal{M}$. The changes in freshwater input due to water cycle changes may be quantified at the surface of the ocean. As with salinity in equations (3) and (4), we begin by quantifying surface freshwater fluxes into volumes bounded by isotherms before interpolating onto temperature-percentiles:

$$\mathcal{F}_s(\Theta^*,t) = \frac{1}{\rho_0} \frac{\partial}{\partial \Theta^*} \left(\frac{\partial \Theta^*}{\partial \mathcal{A}} \right) \iiint_{\Theta(x,y,z,t) > \Theta^*} (P + E + R)\, dxdy;$$
$$\mathcal{F}_s(\Theta^*,t) \Longrightarrow \mathcal{F}_s(\Theta(p,t),t) = \mathcal{F}_s(p,t) \tag{7}$$

where $\mathcal{A}$ is the surface area bounded by contours of temperature Θ^*, ρ_0 is the reference density, assumed to be $\rho_0 = 1035$ kgm^{-3}, and P, E and R are the precipitation, evaporation and river runoff respectively, in kg/s, assumed to be positive into the ocean. The residual between surface freshwater fluxes and the global freshwater flux represents the fluxes of salinity between percentile layers in the ocean.

Data

We explore the salinity tendency and freshwater and water cycle change over 44 years from 1970 to 2014 in a number of observational and climate model data sets.

Observations

The observational results presented come from four observational datasets:

- *IAP Data:* In-situ gridded temperature and salinity observations from [20, 21] for the upper ocean ($z < 2000$ m), monthly-averaged from 1970 to 2014 with 1-degree horizontal resolution.
- *EN4 Data:* Full-depth in-situ temperature and salinity data from the UK Met Office Hadley Centre Enhanced Ocean Data Assimilation and Climate prediction (ENACT) version 4 (subversion EN.4.2.1, with [22] XBT corrections, see [18] for more details), monthly-averaged from 1970 to 2014 with 1-degree horizontal resolution.
- *Ishii Data:* In-situ temperature and salinity data from [17] for the upper ocean ($z < 1500$ m), monthly-averaged from 1970 to 2012 with 1-degree horizontal resolution.
- *Composite Data:* Full-depth composite of IAP data for $z < 2000$ m and EN4 data for $z > 2000$ m, monthly-averaged from 1970 to 2014 with 1-degree horizontal resolution.

Note that the IAP dataset is specifically formulated to reduce errors associated with sampling biases due to the rapid introduction of Argo in the early 2000s (see [21] for more details), so we opt to use it where available. The composite dataset therefore makes use of the IAP data in the upper ocean and fills the deep ocean with EN4 data. All observed temperature and salinity measurements are converted to Conservative Temperature and Absolute Salinity in line with oceanographic standard practice and following recommendations by the UNESCO-IOC [23, 24, 25, 26]. Marginal seas (the Mediterranean, Red, Baltic, and Black Seas, the Persian Gulf and Hudson Bay) are influenced by ocean processes different to the major ocean basins and vary in size and shape between climate models, so are excluded in the observations.

In addition, the time-mean surface freshwater fluxes in the observations are quantified by taking the average of precipitation and evaporation data from four reanalysis products - the Japanese 25 year Reanalysis (JRA-25)/JMA Climate Data Assimilation System (JRA), NCEP/DOE Reanalysis II (NCEP2), ECMWF Interim Reanalysis (ERA-I) and NASA Modern Era Reanalysis for Research and Applications (MERRA) from 1979 to 2011 (see [3] for more information on data sources and binning procedure). Runoff data is obtained from [27], binned onto temperature-percentiles and added to the evaporation and precipitation estimates from JRA, NCEP2, ERA-I and MERRA.

Models

The analysis presented here enables direct comparisons between observations and climate models. We assess the difference between observations and climate models using twenty climate models from the Climate Model Intercomparison Project phase 6 [CMIP6;[28]] (model names and references are provided in the supplementary information, Table S1). We focus on the historical experiments in the CMIP6 models (with masked marginal seas) which branch off from the pre-industrial control (*piControl*) runs from 1850 onwards. We analyse monthly-averaged potential temperature and practical salinity fields from January 1970 to December 2014. Note that the difference between the potential temperature and practical salinity provided in the models and conservative temperature and absolute salinity is negligible [26]. Any differences between the CMIP6 models and observations may be attributed to the forcing field by comparing the CMIP6 response to a set of Detection and Attribution Model Intercomparison Project (DAMIP) models. We look individually at the change in salinity in GHG-only (*hist-GHG*) and AA-only (*hist-aer*) runs in six DAMIP models which branch off from the *piControl* run in 1850. In these runs, the models are separately forced by AAs and GHGs in an effort to attribute the model response to either forcing field (see [29] for more details of the DAMIP protocol). The list of DAMIP models used and relevant references (which include further details on the model setup) may be found in the supplementary information (Table S2). As with the CMIP6 models, the monthly-averaged potential temperature and practical salinity fields from January 1970 to December 2014 are analysed in the DAMIP models.

In the observations, CMIP6 runs and the DAMIP runs, the annual mean of all relevant monthly-averaged variables is calculated, binned into temperature space and interpolated onto temperature-percentiles. The surface freshwater fluxes $\mathcal{F}_s(p,t)$ are then time-integrated. Model drift from the *piControl* experiment is removed using a cubic fit to ensure forced trends are accurately captured [19]. The slope of the linear trend in the binned variable $S(p,t)$ is then used to calculate $\mathcal{F}(p,t)$, and the slope of the linear trend in the time-integrated surface freshwater flux $\int_t \mathcal{F}_s(p,t)dt$ yields the surface freshwater flux anomaly. Surface flux intensification (y-axis in figure 4) is calculated by dividing the surface freshwater flux anomaly by the climatological mean surface freshwater fluxes. Note that surface freshwater flux anomalies are not readily available in observations (with substantial regional variance between atmospheric reanalyses, see [3]), so they are only calculated for the CMIP6 and DAMIP runs.

References

[1] Kevin E. Trenberth, Lesley Smith, Taotao Qian, Aiguo Dai, and John Fasullo. Estimates of the Global Water Budget and Its Annual Cycle Using Observational and Model Data. *Journal of Hydrometeorology*, 8(4):758–769, 2007.

[2] Gabriele C. Hegerl, Emily Black, Richard P. Allan, William J. Ingram, Debbie Polson, Kevin E. Trenberth, Robin S. Chadwick, Phillip A. Arkin, Beena Balan Sarojini, Andreas Becker, Aiguo Dai, Paul J. Durack, David Easterling, Hayley J. Fowler, Elizabeth J. Kendon, George J. Huffman, Chunlei Liu, Robert Marsh, Mark New, Timothy J. Osborn, Nikolaos Skliris, Peter A. Stott, Pier-Luigi Vidale, Susan E. Wijffels, Laura J. Wilcox, Kate M. Willett, and Xuebin Zhang. Challenges in Quantifying Changes in the Global Water Cycle. *Bulletin of the American Meteorological Society*, 96(7):1097–1115, 2015.

[3] Jeremy P Grist, Simon A Josey, Jan D Zika, Dafydd Gwyn Evans, and Nikolaos Skliris. Assessing recent air-sea freshwater flux changes using a surface temperature-salinity space framework. *Journal of Geophysical Research: Oceans*, 121(12):8787–8806, 2016. Grist et al., 2016: Great paper to be cited in future.

[4] Lisan Yu, Simon A. Josey, Frederick M. Bingham, and Tong Lee. Intensification of the global water cycle and evidence from ocean salinity: a synthesis review. *Annals of the New York Academy of Sciences*, 1472(1):76–94, 2020.

[5] Paul J. Durack, Susan E. Wijffels, and Richard J. Matear. Ocean Salinities Reveal Strong Global Water Cycle Intensification During 1950 to 2000. *Science*, 336(6080):455–458, 2012.

[6] Jan D Zika, Nikolaos Skliris, Adam T Blaker, Robert Marsh, A J George Nurser, and Simon A Josey. Improved estimates of water cycle change from ocean salinity: the key role of ocean warming. *Environmental Research Letters*, 13(7):074036, 2018.

[7] Kieran P. Helm, Nathaniel L. Bindoff, and John A. Church. Changes in the global hydrological-cycle inferred from ocean salinity. *Geophysical Research Letters*, 37(18):n/a–n/a, 2010.

[8] Nikolaos Skliris, Jan D. Zika, George Nurser, Simon A. Josey, and Robert Marsh. Global water cycle amplifying at less than the Clausius-Clapeyron rate. *Scientific Reports*, 6(1):38752, 2016.

[9] Isaac M. Held and Brian J. Soden. Robust Responses of the Hydrological Cycle to Global Warming. *Journal of Climate*, 19(21):5686–5699, 2006.

[10] Richard P. Allan, Mathew Barlow, Michael P. Byrne, Annalisa Cherchi, Hervé Douville, Hayley J. Fowler, Thian Y. Gan, Angeline G. Pendergrass, Daniel Rosenfeld, Abigail L. S. Swann, Laura J. Wilcox, and Olga Zolina. Advances in understanding large-scale responses of the water cycle to climate change. *Annals of the New York Academy of Sciences*, 1472(1):49–75, 2020.

[11] Lijing Cheng, Kevin E. Trenberth, Nicolas Gruber, Michael E. Mann, John P. Abraham, John Fasullo, Guancheng Li, Xuanming Zhao, and Jiang Zhu. Ocean salinity changes expose a human fingerprint. 2020.

[12] L. V. Worthington. The Water Masses of the World Ocean:Some Results of a Fine-Scale Census. 1981.

[13] Nikolaos Skliris, Robert Marsh, Simon A. Josey, Simon A. Good, Chunlei Liu, and Richard P. Allan. Salinity changes in the World Ocean since 1950 in relation to changing surface freshwater fluxes. *Climate Dynamics*, 43(3-4):709–736, 2014.

[14] Nathaniel L. Bindoff and Trevor J. Mcdougall. Diagnosing Climate Change and Ocean Ventilation Using Hydrographic Data. *Journal of Physical Oceanography*, 24(6):1137–1152, 1994.

[15] Taimoor Sohail, Damien B. Irving, Jan D. Zika, Ryan M. Holmes, and John A. Church. Fifty Year Trends in Global Ocean Heat Content Traced to Surface Heat Fluxes in the Sub-Polar Ocean. *Geophysical Research Letters*, 48(e2020GL091439):1 – 13, 4 2021.

[16] Lijing Cheng and Jiang Zhu. Benefits of CMIP5 multimodel ensemble in reconstructing historical ocean subsurface temperature variations. *Journal of Climate*, 29(15):5393–5416, 2016.

[17] Masayoshi Ishii, Akiko Shouji, Satoshi Sugimoto, and Takanori Matsumoto. Objective analyses of sea-surface temperature and marine meteorological variables for the 20th century using ICOADS and the Kobe Collection. *International Journal of Climatology*, 25(7):865–879, 2005.

[18] Simon A. Good, Matthew J. Martin, and Nick A. Rayner. EN4: Quality controlled ocean temperature and salinity profiles and monthly objective analyses with uncertainty estimates. *Journal of Geophysical Research: Oceans*, 118(12):6704–6716, 2013.

[19] Damien Irving, Will Hobbs, John Church, and Jan Zika. A Mass and Energy Conservation Analysis of Drift in the CMIP6 Ensemble. *Journal of Climate*, 34(8):3157–3170, 2020.

[20] Lijing Cheng, Kevin E Trenberth, John Fasullo, Tim Boyer, John Abraham, and Jiang Zhu. Improved estimates of ocean heat content from 1960 to 2015. *Science Advances*, 3(3):e1601545, 2017.

[21] Lijing Cheng, Kevin E. Trenberth, Nicolas Gruber, John P. Abraham, John T. Fasullo, Guancheng Li, Michael E. Mann, Xuanming Zhao, and Jiang Zhu. Improved estimates of changes in upper ocean salinity and the hydrological cycle. *Journal of Climate*, 33(23):1–74, 2020.

[22] Viktor Gouretski and Franco Reseghetti. On depth and temperature biases in bathythermograph data: Development of a new correction scheme based on analysis of a global ocean database. *Deep Sea Research Part I: Oceanographic Research Papers*, 57(6):812–833, 2010.

[23] Trevor J. McDougall. Potential Enthalpy: A Conservative Oceanic Variable for Evaluating Heat Content and Heat Fluxes. *Journal of Physical Oceanography*, 33(5):945–963, 2003.

[24] Trevor J. McDougall and Paul M. Barker. Getting started with TEOS---10 and the Gibbs Seawater (GSW) Oceanographic Toolbox. *SCOR/IAPSO WG127*, page 28, 2011.

[25] Felicity S. Graham and Trevor J. McDougall. Quantifying the Nonconservative Production of Conservative Temperature, Potential Temperature, and Entropy. *Journal of Physical Oceanography*, 43(5):838–862, 2013.

[26] Trevor J. McDougall, Paul M. Barker, Ryan M. Holmes, Rich Pawlowicz, Stephen M. Griffies, and Paul J. Durack. The interpretation of temperature and salinity variables in numerical ocean model output, and the calculation of heat fluxes and heat content. *Geoscientific Model Development Discussions*, 2021:1–48, 2021.

[27] Aiguo Dai. Dai and Trenberth Global River Flow and Continental Discharge Dataset, 2017.

[28] Veronika Eyring, Sandrine Bony, Gerald A. Meehl, Catherine A. Senior, Bjorn Stevens, Ronald J. Stouffer, and Karl E. Taylor. Overview of the Coupled Model Intercomparison Project Phase 6 (CMIP6) experimental design and organization. *Geoscientific Model Development*, 9(5):1937–1958, 2016.

[29] Nathan P. Gillett, Hideo Shiogama, Bernd Funke, Gabriele Hegerl, Reto Knutti, Katja Matthes, Benjamin D. Santer, Daithi Stone, and Claudia Tebaldi. The Detection and Attribution Model Intercomparison Project (DAMIP v1.0) contribution to CMIP6. *Geoscientific Model Development*, 9(10):3685–3697, 2016.

Supplementary Files

This is a list of supplementary files associated with this preprint. Click to download.

- NFWpaperSI.pdf